

1 Impact of UV irradiation on multiwall carbon
2 nanotubes in nanocomposites: formation of
3 entangled surface layer and mechanisms of release
4 resistance

5 Tinh Nguyen, Elijah J. Petersen*, Bastien Pellegrin¹, Justin M. Gorham, Thomas Lam, Minhua
6 Zhao², Lipiin Sung*

7 National Institute of Standards and Technology (NIST), Gaithersburg, Maryland 20899

8 ¹*Current address: Steap Stailor, Rue Dr Schweitzer, 38180 SEYSSINS - FRANCE*

9 ²*Current address: X-wave Innovations, Inc., Gaithersburg, MD 20878, United States*
10

11

12 *Corresponding authors: lipiin@nist.gov; elijah.petersen@nist.gov
13
14
15

16 **Abstract**

17 Multiwall carbon nanotubes (MWCNTs) are nanofillers used in consumer and structural
18 polymeric products to enhance a variety of properties. Under weathering, the polymer matrix will
19 degrade and the nanofillers may be released from the products potentially impacting ecological or
20 human health. In this study, we investigated the degradation of a 0.72 % (by mass)
21 MWCNT/amine-cured epoxy nanocomposite irradiated with high intensity ultraviolet (UV) light
22 at various doses, the effects of UV exposure on the surface accumulation and potential release of
23 MWCNTs, and possible mechanisms for the release resistance of the MWCNT surface layer
24 formed on nanocomposites by UV irradiation. Irradiated samples were characterized for chemical
25 degradation, mass loss, surface morphological changes, and MWCNT release using a variety of
26 analytical techniques. Under 295 nm to 400 nm UV radiation up to a dose of 4865 MJ/m², the
27 nanocomposite matrix underwent photodegradation, resulting in formation of a dense, entangled
28 MWCNT network structure on the surface. However, no MWCNT release was detected, even at
29 very high UV doses, suggesting that the MWCNT surface layer formed from UV irradiation of
30 polymer nanocomposites resist release. Four possible release resistance mechanisms of the UV-
31 induced MWCNT surface layer are presented and discussed.

32

33 **1. Introduction**

34 Nanocomposites, materials containing a nanofiller (defined as any particle with a
35 characteristic dimension between 1 nm and 100 nm) incorporated into the matrix material (*e.g.*,
36 polymer, ceramic), often have novel or enhanced properties as compared to the unmodified matrix
37 material [1]. For nanocomposites incorporating multiwall carbon nanotubes (MWCNTs), these
38 changes may include enhanced mechanical strength, flame retardant capacities, or electrical
39 properties [2, 3], advantages that have or may result in potential applications in aerospace [4],
40 construction [5], and consumer products [6].

41 For widespread market adoption of nanocomposites, it is important to understand if the
42 nanofillers might have any adverse impacts. This could occur if environmental stresses (*e.g.*,
43 biodegradation, ultraviolet (UV) light, and moisture) cause release of the nanofiller [6-18].
44 MWCNTs are one nanofiller of concern for potential environmental and/or human health effects
45 due to its high aspect ratio [7, 19-24]. There have been a number of studies conducted to date on
46 release of MWCNTs due to mechanical stresses (*e.g.*, abrasion, sanding, polishing) [1, 23, 25-35],
47 yet fewer on the fate and release caused by environmental stresses [14, 17, 23, 31, 32, 36]. Recent
48 studies on the potential toxicological effects of materials released from MWCNT nanocomposites
49 have not shown increased toxicity compared to particles released from the polymer matrix under
50 the environmental conditions tested [14, 23, 32, 33]. While release of individual MWCNT from
51 nanocomposites has been detected in a few studies after abrasion [23, 30, 33] or sanding [29], most
52 studies have not found detectable MWCNT release by exposures to weathering environments [13,
53 25-28, 31, 32, 35]. In fact, numerous studies have shown MWCNT accumulation on the
54 nanocomposite surface after exposures to UV radiation [14, 17, 28, 31, 32, 37], the most dominant
55 weathering element known to cause severe degradation of polymeric materials used outdoors [38].

56 The factors that cause MWCNT agglomeration and network formation on the surface are not yet
57 well understood. In a previous study at a high MWCNT loading (3.5 % mass fraction based on the
58 polymer solid matrix; all percentages in this study refer to a mass percentage of MWCNTs in the
59 composite materials), we have observed a strong photostabilization effect of the epoxy matrix by
60 MWCNT and a measurable quantity of MWCNT accumulated on the nanocomposite surface after
61 exposure to UV radiation [37]. The impacts of UV irradiation on nanocomposites containing much
62 lower MWCNT loadings are not known. Further, the main focus of the previous work was to
63 develop methodologies for characterizing surface chemistry changes of the nanocomposites
64 resulting from UV exposure, without any attempts to measure MWCNTs released from the
65 irradiated nanocomposite.

66 In this study, we have investigated, using a suite of analytical methods developed and
67 applied in our previous publication [37], the dose-dependent effects of UV irradiation on the
68 degradation, surface accumulation, and potential for nanofiller release from nanocomposites
69 containing a one-fifth of the MWCNT loading than previously studied, namely a 0.72 % MWCNT
70 epoxy nanocomposite sample compared to the previously tested 3.5 % MWCNT epoxy
71 nanocomposite sample. The results of this and previous experiments will provide essential data to
72 assess the role of MWCNT concentration on the impact of UV radiation on MWCNT surface
73 accumulation and release potential from a polymer nanocomposite. These experiments were
74 conducted via accelerated aging using intense UV radiation with the same spectral regime as the
75 UV portion of natural sunlight (295 nm to 400 nm) at elevated temperature (50 °C) and humidity
76 (75 % relative humidity) in the National Institute of Standards and Technology (NIST) SPHERE
77 (Simulated Photodegradation via High Energy Radiant Exposure) [39]. Based on our experimental
78 results, which showed severe degradation of the matrix and a substantial MWCNT surface

79 accumulation at both MWCNT loading concentrations but without an apparent release after a very
80 high UV dose (4865 MJ/m², i.e., 9-month exposure), we present four potential mechanisms to
81 explain the strong release resistance of the MWCNT surface layer formed on nanocomposites by
82 UV irradiation. However, additional mechanical and environmental stresses to the nanocomposite
83 after UV irradiation could also potentially result in release during the use, disposal, or recycling
84 of MWCNT nanocomposites [34, 35, 40].

85 **2. Experimental Section**

86 *2.1. Materials and Sample Preparation*

87 Epoxy nanocomposite films containing a 0.72 % mass fraction of MWCNTs were used in
88 this study. The matrix was a stoichiometric mixture of a diglycidyl ether of bisphenol A (DGEBA)
89 epoxy resin having an equivalent mass of 189 and a polyoxypropylenetriamine curing agent. The
90 epoxy matrix was used without UV stabilizers or additives. MWCNT was a commercial 1 % mass
91 fraction pre-dispersed product in the same epoxy resin. To better understand the starting material,
92 the sizes of the MWCNT were investigated using scanning electron microscopy (SEM) after
93 extraction from the epoxy resin using a toluene extraction procedure described previously [37].
94 The estimated average MWCNT diameter was 20.5 nm with a standard deviation of 4.0 nm
95 (n=200), and the lengths predominately ranged between 200 nm and 2 μm; challenges associated
96 with accurately obtaining a MWCNT length distribution have been previously described [41].
97 SEM micrographs and a histogram of the MWCNT diameters are provided in Figure S1.

98 Free-standing films of unfilled epoxy (neat) and 0.72 % MWCNT epoxy composite were
99 fabricated (note that the 1% mass fraction MWCNT in the epoxy resin is reduced to 0.72 % mass
100 fraction in the amine-cured epoxy). Neat epoxy and MWCNT epoxy nanocomposite films were
101 prepared by adding appropriate amounts of amine curing agent directly to the epoxy resin or the

102 MWCNT pre-dispersed epoxy resin, respectively, and stirring for 1 h with a magnetic stirrer. After
103 degassing for 1 h at room temperature, the epoxy/amine/MWCNT mixture was drawn down on a
104 polyethylene terephthalate sheet attached to a vacuum table using a bar applicator to produce free
105 standing films having a thickness of approximately 150 μm (cross sectional analysis performed by
106 laser scanning confocal microscopy). Reagent grade toluene (purity > 99.5 %) was used for all
107 composite processing. All coated samples were cured at ambient conditions (24 °C and 45 %
108 relative humidity) for three days, followed by post-curing at 110 °C for 4 h in an air circulating
109 oven. The dispersion of MWCNTs in the amine-cured epoxy matrix was good, as shown by SEM
110 cross section imaging presented elsewhere [42].

111 *2.2. UV Irradiation*

112 UV irradiation of neat epoxy and MWCNT epoxy nanocomposite films was performed
113 using a NIST-developed 2 m SPHERE [39] as previously described [37]. This SPHERE UV
114 chamber utilizes a mercury arc lamp system that produces a collimated and highly uniform UV
115 flux of approximately 140 W/m^2 in the UVB and UVA (295 nm to 400 nm) range, which is the
116 most detrimental range on polymer degradation. Although the spectrum of this light source
117 contains some radiation having wavelength in the visible range (Figure S2), previous studies [43,
118 44] on wavelength effect indicated that the degradation of epoxy caused by radiation > 400 nm is
119 very small (<1 % of UVB region). In addition, previous results from our laboratory have shown
120 similar degradation mechanisms for multiple experimental conditions between epoxy samples
121 degraded in the NIST SPHERE and in the outdoor environment [43]. The stability of this light
122 source during the experiment was evaluated, and it was shown that there was essentially no change
123 in radiation intensity in the 295 nm to 400 nm region after three months of exposure (Figure S2).
124 It can also precisely control the relative humidity (RH) and temperature. In this study, 25 mm x 25

125 mm specimens were exposed in the SPHERE UV chamber at 50 °C and 75 % RH. Importantly,
126 the choice to run the experiments at 50 °C was made to increase the degradation rate and also
127 because we have observed that the temperature on composite surfaces during summer outdoor
128 exposure often reaches 50 °C or higher even if the ambient temperature in the environment is
129 lower. Specimens were removed at specified UV doses for various characterizations. For assessing
130 the release of MWCNTs, specimens having a surface area of approximately 78.5 cm² and a
131 specially-designed sample holder described previously [9] were employed. This holder consisted
132 of a sample chamber, inlet and outlet to supply humid air to the irradiated specimen, and collectors
133 placed at the bottom of the holder to collect any released particles. A cover made of quartz that
134 allows UV radiation transmitted through and irradiated the specimen was used to seal the holder.
135 A humidity sensor was placed inside the sample holder to monitor RH of the exposure
136 environment. Three types of material having a dimension of approximately 5 mm x 5mm were
137 placed on the collector surface: white poly(tetrafluoroethylene) film, highly polished silicon plate,
138 and conductive tape. The surface of all three liners were analyzed after UV irradiation. A picture
139 of the MWCNT-release assessment holder containing a 0.72 % MWCNT epoxy nanocomposite
140 specimen is displayed in Figure S3.

141 *2.3 Characterization of UV-irradiated Nanocomposites*

142 Mass loss, chemical degradation, surface morphological changes, and release of MWCNTs
143 from UV-irradiated specimens were characterized as a function of UV dose. Mass loss was
144 measured using an analytical balance (Mettler Toledo AB265-S, Columbus, OH) having a
145 resolution of 10⁻⁵ g, and is expressed as: $(M_t - M_0)/M_0 \times 100$, where M_t is the specimen mass at
146 irradiation time t , M_0 is the specimen mass before irradiation. Chemical degradation was measured
147 with Fourier transform infrared spectroscopy in the attenuated total reflection mode (FTIR-ATR)

148 and X-ray photoelectron spectroscopy (XPS). FTIR-ATR spectra were recorded at a resolution of
149 4 cm^{-1} using dry air as a purge gas and a spectrometer equipped with a liquid nitrogen-cooled
150 mercury cadmium telluride (MCT) detector. All spectra were the average of 128 scans. The peak
151 height was used to represent the infrared intensity, which is expressed in absorbance, A. All FTIR
152 results were the average of four specimens. XPS measurements were performed on an Axis Ultra
153 DLD spectrophotometer using 150 W (10 mA, 15 kV) monochromatic, Al $K\alpha$ X-rays with
154 photoelectrons collected along the surface normal at 20 eV pass energy. Photoelectrons were
155 counted at 0.050 eV steps for 500 ms/step and 2 sweeps. XP spectra of the C (1s) region were
156 taken without charge neutralization for detection of MWCNT surface enhancement, and spectra
157 for semi-quantitative elemental analysis were acquired with charge neutralization. Spectral
158 analysis was conducted using CasaXPS with Tougaard backgrounds fitted to each C (1s) region
159 regardless of the conditions the spectra were acquired. Elemental analysis on neutralized spectra
160 also factored in contributions from O (1s) and N (1s) from the epoxy matrix as well as Na, Ca and
161 Si contaminants, each of which was fitted with a Shirley background. Elemental percentages are
162 based on the peak area corrected with an elemental sensitivity factor of 1.685, 0.78, 0.477, 1.833,
163 0.278 and 0.328 for the Na (1s), O (1s), N (1s), Ca (2p), C (1s) and Si (2p) regions, respectively,
164 as provided by the manufacturer. Contaminants are not shown in the results; however, Na, Ca,
165 and Si were each $< 1\%$ of the elemental percentages with the exception of the two highest UV
166 doses, which had silicon at 1.8 % and 5.5 %, respectively. Plotted data points are representative
167 of the average of at least 3 measurements at different locations and the error bars represent one
168 standard deviation.

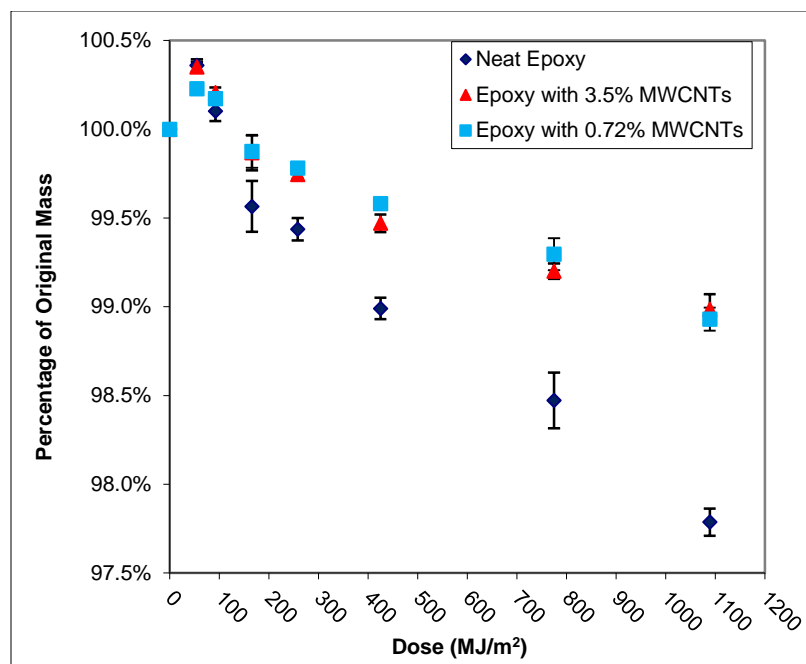
169 Surface morphological changes were characterized by scanning electron microscopy
170 (SEM), atomic force microscopy (AFM), and electric force microscopy (EFM). The potential for

171 MWCNT release after irradiation for 4865 MJ/m^2 (i.e., 9 months of exposure) was examined by
172 SEM imaging of the surface of all three collector liners. SEM analysis was performed using a Zeiss
173 Supra-55VP Field Emission SEM. A 5 kV acceleration voltage was used for the surface analysis
174 of the nanocomposites and acceleration voltages over 15 kV were applied during cross sectional
175 analysis of the samples prepared by freeze fracture. As mentioned previously [37], the higher
176 acceleration voltage allows for the visualization of MWCNT morphology within the embedded
177 matrix by charge contrast imaging. Detailed procedures for AFM and EFM measurements were
178 described previously [45]. Briefly, the conventional height and phase images were acquired in
179 normal tapping mode using a Veeco Dimension 3100 atomic force microscope while the EFM
180 images were obtained under lift-mode using a conductive AFM probe with an applied bias voltage
181 ranging between -12 V and $+12 \text{ V}$.

182 **3. Results and Discussion**

183 *3.1. Effects of UV Irradiation on Bulk Material*

184 The mass loss of neat epoxy and 0.72 % and 3.5 % MWCNT epoxy nanocomposite samples as a
185 function of UV dose in the NIST SPHERE was measured (Figure 1). The results for the neat epoxy
186 and 3.5 % MWCNT nanocomposite were presented previously [37] and are included in this figure
187 for comparison. All samples showed a small increase in mass at the lowest UV dosages. This result
188 was likely due to moisture uptake when the samples were transferred from the 45 % RH ambient
189 condition to the 75 % RH of the exposure chamber, causing a greater mass gain than mass loss
190 from nanocomposite degradation.



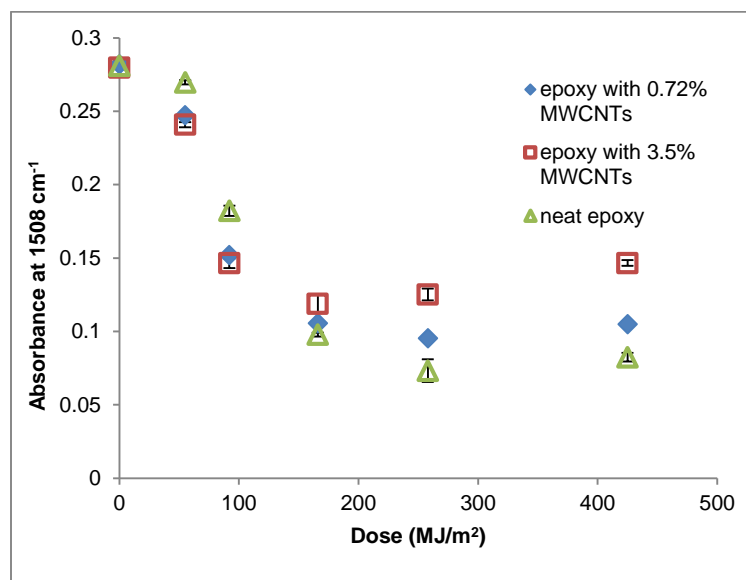
191
 192 **Figure 1.** Remaining mass as a function of dose for neat epoxy, 0.72 % MWCNT epoxy
 193 nanocomposite samples, and 3.5 % MWCNT epoxy nanocomposite samples exposed to UV
 194 radiation at 50 °C and 75 % relative humidity. Data for the neat epoxy and 3.5 % MWCNT epoxy
 195 nanocomposite samples is taken from Reference 37 with permission from Carbon. Results are the
 196 average of five specimens (except for the 775 MJ/m² and 1089 MJ/m² samples for the neat epoxy
 197 for which n=4), and error bars represent one standard deviation.

198
 199 For all samples, the mass loss increased as the UV dose increased; however, the MWCNT
 200 nanocomposite samples consistently had less mass loss than the neat epoxy samples. The rate of
 201 mass loss for the two MWCNT epoxy nanocomposites loadings was nearly identical. Since CNTs
 202 have been shown to photostabilize polymers by mainly radiation screening [46], this result
 203 suggests that the screening of UV radiation by the MWCNTs was not substantially impacted by
 204 the MWCNT concentration in the range of 0.7 % to 3.5 %.

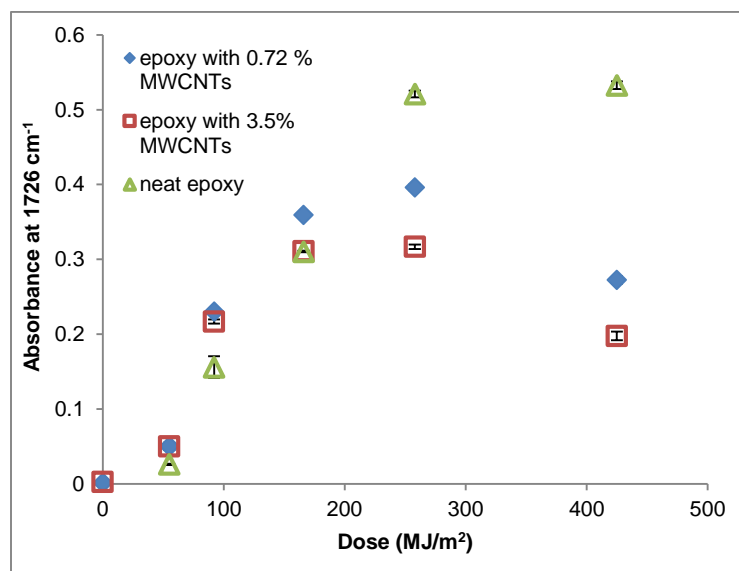
205 3.2. *Effects of UV Irradiation on Nanocomposite Surface Chemistry*

206 Figure 2 shows the FTIR-ATR results from the neat epoxy and MWCNT epoxy
207 nanocomposites samples after UV irradiation. We have described the results for the neat epoxy
208 and 3.5 % MWCNT nanocomposite samples previously [37]. Thus, this discussion will focus on
209 comparing the results for the 0.72 % MWCNT nanocomposite sample to the other two samples at
210 two key IR bands: 1508 cm^{-1} (due to benzene ring) of the epoxy structure and 1726 cm^{-1} (attributed
211 to aldehyde/ketone C=O stretching) formed during UV irradiation. Changes in the 1508 cm^{-1} and
212 1726 cm^{-1} bands represent chain scission and photo-oxidation, respectively. The full difference
213 FTIR-ATR spectra for the 0.72 % MWCNT nanocomposite sample are provided in Figure S4.
214 Both MWCNT nanocomposite samples and the neat epoxy showed rapid degradation under this
215 UV/RH/T environment with a similar decrease of the 1508 cm^{-1} band and increase of the 1726 cm^{-1}
216 band between 0 MJ/m^2 and 166 MJ/m^2 . This result suggests that the degradation rate of the matrix
217 surface layer ($< 2.5 \mu\text{m}$, [37]) in this dose range (i.e., early stage of degradation) was independent
218 of the MWCNT loading. For both MWCNT epoxy nanocomposites, these changes reached a
219 plateau at approximately 166 MJ/m^2 dose, but they continued to advance until 270 MJ/m^2 dose for
220 the neat epoxy. Further, the difference in the level of degradation between the three materials was
221 well separated between 166 MJ/m^2 and 425 MJ/m^2 . In this range, the 0.72 % CNT composite
222 exhibited a greater degradation than the 3.5 % composite did, likely due to the stronger shielding
223 effect by the larger amount of CNTs accumulated on the surface of the latter. As described
224 previously [37], the intensity decrease of the band at 1726 cm^{-1} at the highest dose for both
225 MWCNT nanocomposite samples is probably due to the substantial accumulation of MWCNT on
226 the sample surface (as shown by SEM and EFM images in a later section), which would decrease
227 the ATR probing depth in the oxidized epoxy layer. In addition, the rough surface topography of

228 the photodegraded MWCNT nanocomposite samples likely decreased the sample-ATR probe
229 contact (hence intensity) and the band intensity of the epoxy matrix.



230



231

232

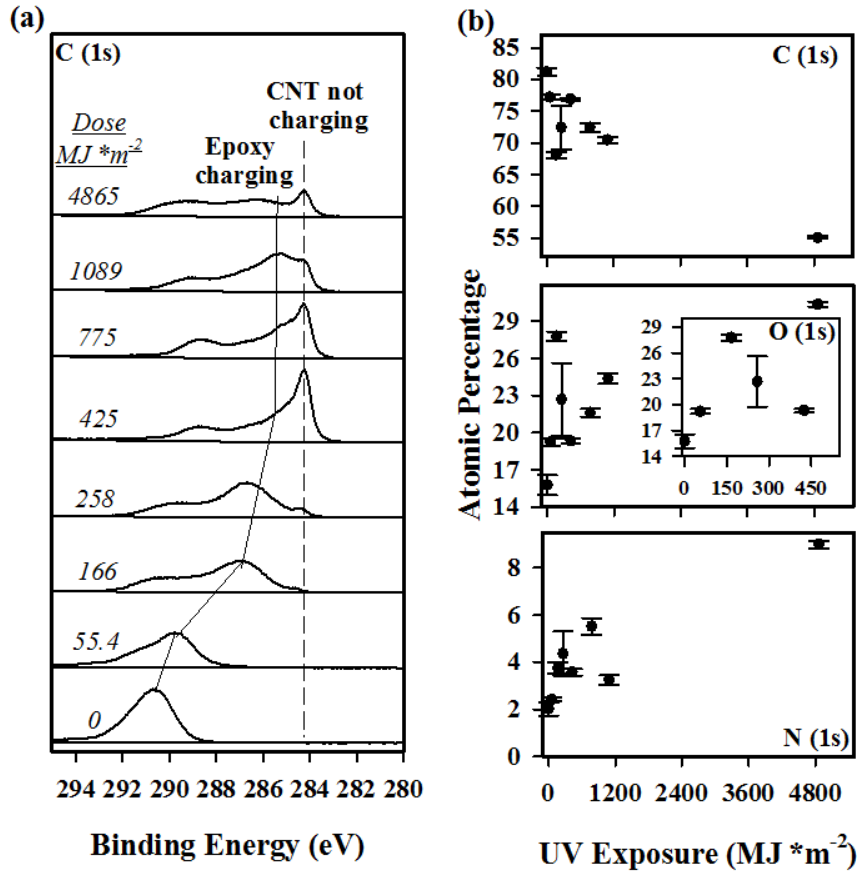
233 **Figure 2.** Changes in FTIR-ATR intensity for (upper) 1508 cm⁻¹ and (lower) 1726 cm⁻¹ bands for
234 neat epoxy, 0.72 % MWCNT epoxy nanocomposite samples, and 3.5% MWCNT epoxy
235 nanocomposite samples before and after UV irradiation with varying doses. Data for the neat
236 epoxy and 3.5 % MWCNT epoxy nanocomposite samples is taken from Reference 37 with

237 permission from Carbon. Each data point was the average of three specimens, and the error bars
238 represent one standard deviation.

239 XPS analysis was applied to answer two questions: (a) are MWCNTs accumulating on the
240 surface by UV irradiation in low MWCNT loading nanocomposites and (b) how does high
241 intensity UV irradiation at very high doses impact the overall surface oxidation? To answer the
242 first question, we evaluated a stack plot of representative, unneutralized C (1s) spectra at each UV
243 dose, as presented in Figure 3(a). The spectral profiles are composed of two differentially charging
244 regions. The first region is reflective of the positively-charged epoxy region at higher binding
245 energies, which is the only feature in the spectra of the unexposed composite and decreases in
246 binding energy with increasing UV dose. The second region, which only became evident after a
247 sufficient dose of UV radiation ($\approx 166 \text{ MJ/m}^2$), is located at a static binding energy of $\approx 284.5 \text{ eV}$
248 and is attributed to the conductive MWCNT mats that formed due to UV-induced removal of the
249 surface epoxy contributions, as has been observed previously [37, 47]. In contrast with previous
250 studies, after the C (1s) regions have reached a MWCNT-like state (dose $\approx 425 \text{ MJ/m}^2$), the XP
251 spectra continued to evolve suggesting that the surface of the nanocomposite continued to be
252 modified. One possibility is that the MWCNTs themselves were increasingly oxidized by the UV
253 radiation.

254 To understand how increased UV dose impacts surface oxidation, the composite's
255 elemental contributions for the C (1s), N (1s), and O (1s) XP spectral regions measured from
256 neutralized spectra were studied (See Figure 3(b)). Over the course of the 4865 MJ/m^2 UV dose
257 irradiation, the surface carbon concentration decreased while the oxygen and nitrogen
258 contributions increased as clearly indicated by the data for the samples exposed for 4865 MJ/m^2 .
259 In the early stage of irradiation, however, there was some variation in the overall trend which can

260 be more easily observed in the inset for the O (1s) plot. At low doses, the O (1s) surface
 261 concentration increased until it reached a value of $(27.8 \pm 0.4) \%$ at $\approx 166 \text{ MJ/m}^2$.



262
 263 **Figure 3.** (a) Representative C(1s) spectra at different UV doses acquired in the absence of charge
 264 neutralization for the 0.72 % MWCNT epoxy nanocomposite samples. Electron vacancies lead to
 265 unfilled, positively charged orbitals resulting in a surface characterized by a peak shifted to higher
 266 binding energies (epoxy charging) and the conductive MWCNTs begin to surface accumulate
 267 around 166 MJ/m^2 . (b) Elemental analysis of the 3 dominant elements from separate XP spectra
 268 acquired under charge neutralization. The O (1s) region has an inset representative of the first
 269 500 MJ/m^2 . Plotted data points are representative of the average of at least 3 measurements at
 270 different locations and the error bar represent one standard deviation.

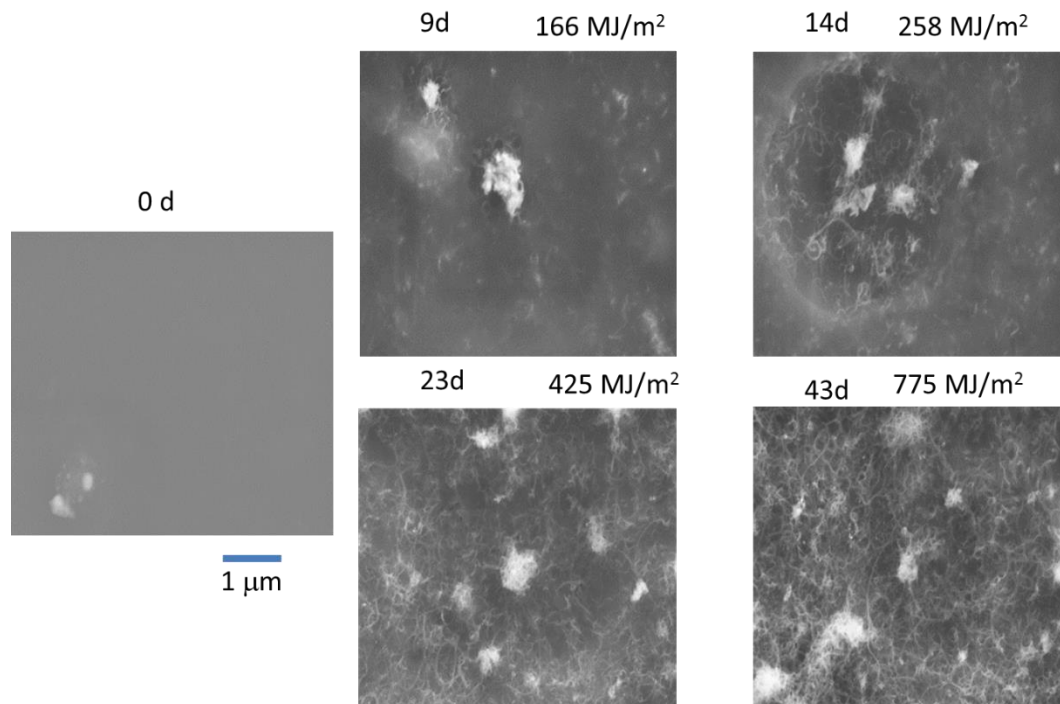
271

272 The oxygen content then decreased to $(19.3 \pm 0.2) \%$ at $\approx 425 \text{ MJ/m}^2$, after which it resumed its
273 increase, albeit at a lower rate. The carbon content followed an inverse trend, first decreasing in
274 percent contributions followed by a switch to increasing at $\approx 166 \text{ MJ/m}^2$, and lastly changing to a
275 decrease at $\approx 425 \text{ MJ/m}^2$. One possible explanation for this behavior is that the outermost surface
276 layer, composed mostly of epoxy, was oxidized as a result of irradiation, raising the surface oxygen
277 content. Once the oxidized epoxy was degraded, the MWCNTs increased in surface concentration,
278 resulting in a corresponding decrease in the oxygen content. This is consistent with the FTIR-ATR
279 observations in Figure 2, which shows an initial gain in C=O functionality at 1726 cm^{-1} followed
280 by a gradual loss in roughly the same doses as observed by XPS. The MWCNTs, which are more
281 resistant to UV-induced oxidation, would subsequently be oxidized at a lower rate.

282 *3.3 Effects of UV Irradiation on Nanocomposite Surface Morphology*

283 The evolution of surface morphology of the 0.72 % MWCNT epoxy nanocomposite with
284 UV irradiation dose is displayed in the SEM images (Figure 4). Very few MWCNTs were visible
285 on the surface of the unexposed sample, but MWCNTs had appeared after 166 MJ/m^2 dose (9 d).
286 The concentration of MWCNTs on the sample surface increased with increasing dose until they
287 mostly covered the surface for all samples exposed to a dose of at least 775 MJ/m^2 . At this point,
288 the MWCNTs have formed a dense layer on the nanocomposite surface. This observation is
289 consistent with results from AFM and EFM imaging (Figure 5), which also revealed that the UV-
290 irradiated surface was mostly covered with MWCNTs after irradiation to the same dose. Figure 5
291 also showed that EFM technique, in particular the EFM phase mode, can provide a stronger
292 contrast of MWCNTs on the surface of nanocomposites than that by the AFM technique. This

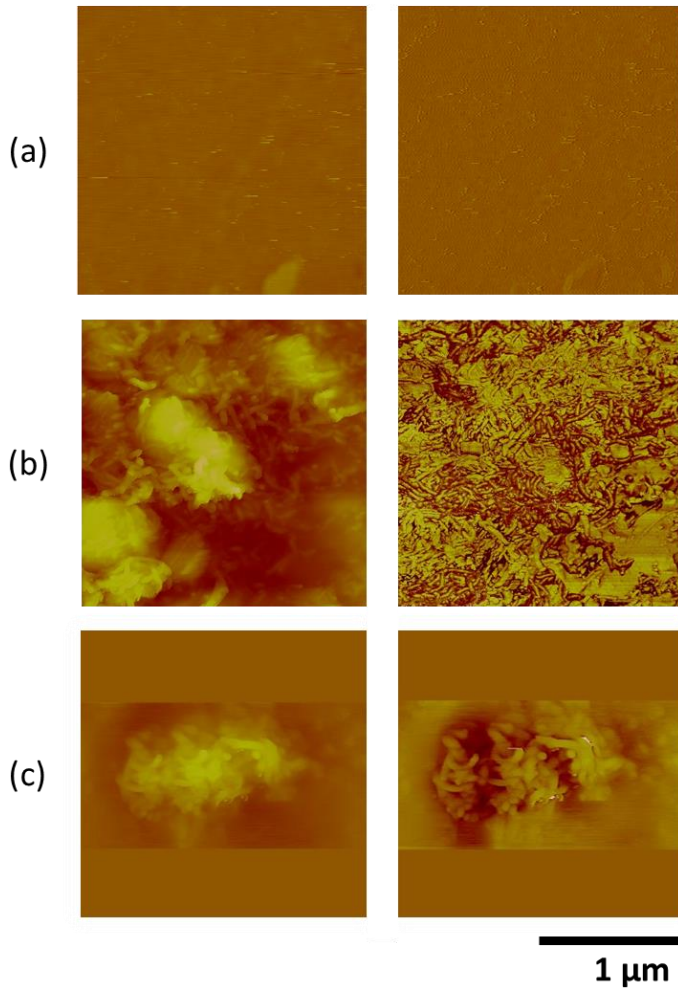
293 observation is consistent with a previous study on characterization of single-walled CNTs
294 (SWCNTs) embedded in a polymer matrix [45]. From the microscopic results (Figures 4 and 5)
295 and spectroscopic data (Figures 2 and 3), it is suggested that the increased MWCNT concentration
296 on the nanocomposite surface with increasing UV irradiation dose was a result of the matrix
297 degradation. As the epoxy matrix near the surface underwent photodegradation and was gradually
298 degraded, MWCNTs in the nanocomposite were increasingly exposed on the surface [15, 48].
299 Overall, the results with the 3.5 % and 0.72 % MWCNT epoxy nanocomposite samples yielded
300 similar results with a thick MWCNT surface layer being formed despite the substantial difference
301 in the MWCNT loading of the initial nanocomposite samples. Similar MWCNT surface
302 accumulation has also been observed for nanocomposites exposing to UV radiation in dry or wet
303 environments [14, 17, 28, 32, 37].



304

305 **Figure 4.** SEM images of 0.72 % MWCNT epoxy nanocomposite before and after UV irradiation
306 at various doses. The scale bar is 1 μm .

307

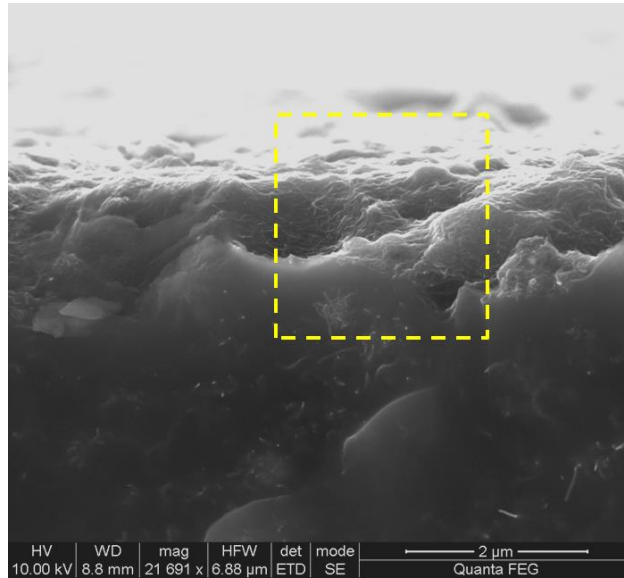


308

309 **Figure 5.** AFM and EFM height and phase images of 0.72 % MWCNT epoxy nanocomposite
310 surface before and after UV irradiation; a): AFM images before irradiation, b) AFM images after
311 irradiation at 775 MJ/m² dose, and c) EFM images after irradiation at 775 MJ/m². Scan size is
312 2 μm . For each pair, height image is on the left and phase image is on the right. The height range
313 of the image is roughly from 0 nm to 800 nm.

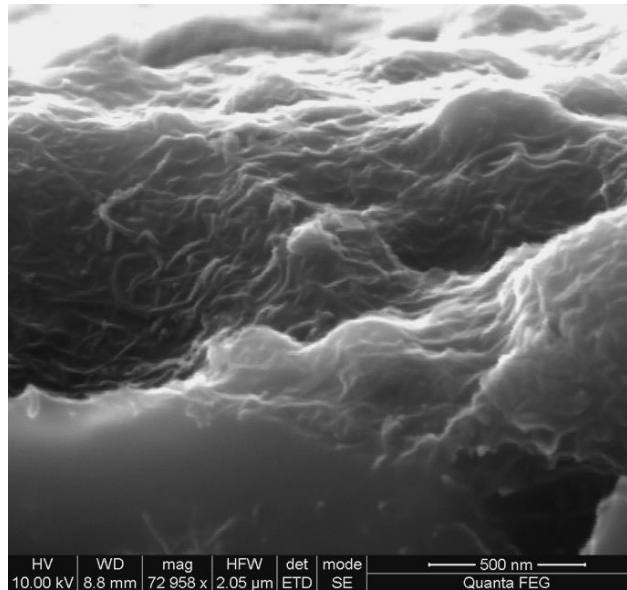
314

315 SEM analysis of cross sections was also carried out to investigate the surface topography
316 of the UV-irradiated 0.72 % MWCNT epoxy nanocomposite samples at 4865 MJ/m² dose. The
317 SEM images showed the formation of a MWCNT surface layer on the sample (Figure 6). In a



2 µm

318



500 nm

319 **Figure 6.** SEM cross section images after 4865 MJ/m² dose (top) and at high
320 magnification(bottom) for the 0.72 % MWCNT epoxy nanocomposite samples.
321

322

323 previous study, the electrical conductivity of the MWCNT surface layer after UV degradation was
324 found to be five times greater than that of the bulk 3.5 % MWCNT nanocomposite [49]. A roughly
325 similar thickness of the MWCNT surface layer was observed after UV irradiation in this study for
326 two doses: 775 MJ/m² (data not shown) and a much higher dose of 4865 MJ/m². This finding
327 suggests that the MWCNT surface layer was effectively shielding the epoxy matrix underneath
328 from further degradation, thus limiting growth in the thickness of the MWCNT surface layer.
329 Based on experimental evidence, theory, and simulation, the high electrical conductivity MWCNT
330 surface layer formed by UV irradiation has been postulated as due to a combination of matrix
331 removal and densification of the MWCNT-rich domains in the nanocomposites [49].

332 It is noted that the substantial amount of MWCNTs formed on the UV irradiated
333 nanocomposite surface observed in this study was from an un-stabilized, model amine-cured
334 epoxy matrix containing aromatic chromophores and electron rich N atoms in the polymer main
335 chains. This epoxy material is known to degrade readily under UV irradiation. For commercial
336 epoxies where UV stabilizers are usually incorporated, the rate of matrix degradation during the
337 early stage of exposure is low and it is expected that little or substantially fewer CNTs would be
338 located on the nanocomposite surface. However, in prolonged exposure (duration depends on
339 concentration and efficacy of the stabilizers) when the amount of UV stabilizers has been
340 substantially decreased or depleted due to both photodegradation and physical leaching, the
341 degradation of the matrix is increased, and it is expected that significant MWCNT would be
342 formed on the nanocomposite surface as observed in this study.

343 *3.4. Mechanisms of Release Resistance of the MWCNT Surface Layer*

344 In addition to measuring the matrix degradation and surface morphological changes, which
345 assessed removal of the epoxy surrounding the MWCNTs, this study also assessed the possibility
346 of MWCNT release caused by the UV irradiation of nanocomposite. This was performed by SEM
347 imaging at high magnification the surfaces of the three liners placed at the bottom of the sample
348 holder (Figure S3) after UV irradiating a 0.72 % MWCNT epoxy nanocomposite specimen having
349 a surface area of 78.5 cm² for 4865 MJ/m² dose (9-month exposure) using the same SPHERE UV
350 chamber. Despite a thick MWCNT surface layer formed on the nanocomposite surface (Figures
351 4,5,6), the result showed no evidence of either nanocomposite fragments or individual MWCNT
352 on the collector surfaces. This result is in contrast to those from nanocomposites of the same epoxy
353 matrix containing spherical nanosilica. In experiments on these composites, substantial
354 nanocomposite fragments and individual silica nanoparticles were found on the collector surface
355 after irradiating the same size sample exposed to the same UV source for 775 MJ/m² dose [9]. This
356 lack of MWCNT spontaneous release (i.e., without applied mechanical forces) observed in this
357 study is similar to that reported previously for other polymer MWCNT composites exposed to
358 weathering environments [14, 17, 28, 32, 37]. It is also in line with other studies that reported a
359 small release amount but only after subjecting the irradiated samples to high shear forces [31] or
360 water spraying [17]. Except under very high shear [31], where some free standing MWCNTs were
361 observed, most of the release fragments under severe mechanical stresses contained MWCNTs
362 embedded in, or protruded from, the matrices. Additionally, by the use of a probe in an AFM
363 instrument, our previous study has demonstrated that the UV irradiation-induced MWCNT surface
364 layer is more resistant to scratching than the neat epoxy matrix [37]. In summary, the results of the
365 present study and those from the literature strongly suggest that, in the absence of strong applied
366 mechanical forces, the MWCNTs formed on the surface of polymer nanocomposites after exposure

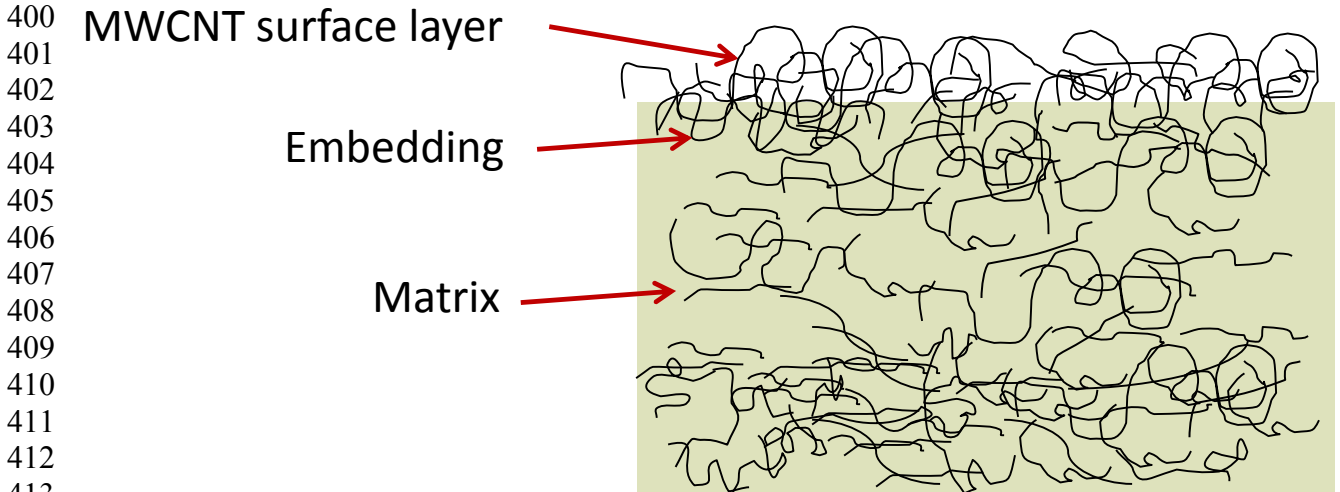
367 to weathering environments or UV radiation are unlikely to be released. It should be noted that the
368 observation of a lack of spontaneous release of MWCNTs after UV irradiation of nanocomposites
369 was studied for only a high aspect ratio MWCNT in a model, unstabilized thermoset epoxy matrix
370 that has a good adhesion with this carbon nanofiller and is known susceptible to degradation by
371 the weathering environments. Additional research is needed on the potential release of MWCNTs
372 having low aspect ratios in more hydrophobic thermoplastic matrices, such as polyolefins, to
373 provide essential data for a more complete assessment of the release of MWCNTs from
374 nanocomposites exposed to UV radiation or weathering conditions. Further investigation is also
375 needed on the effects of mechanical stresses, such as abrasion, and environmental stresses such as
376 free-thaw cycles or hail storms, on the potential rerelease of MWCNTs during UV irradiation or
377 weathering of nanocomposites. Nevertheless, given the lack of evidence of spontaneous release
378 (no applied external stresses) after irradiating to a very high dose of UV radiation or for a long
379 time at high UV intensity, we propose the following plausible mechanisms to explain the strong
380 release resistance of individual MWCNT from the UV- or weather-induced MWCNT surface
381 layer.

382 *3.4.1. Embedded CNTs in Matrix*

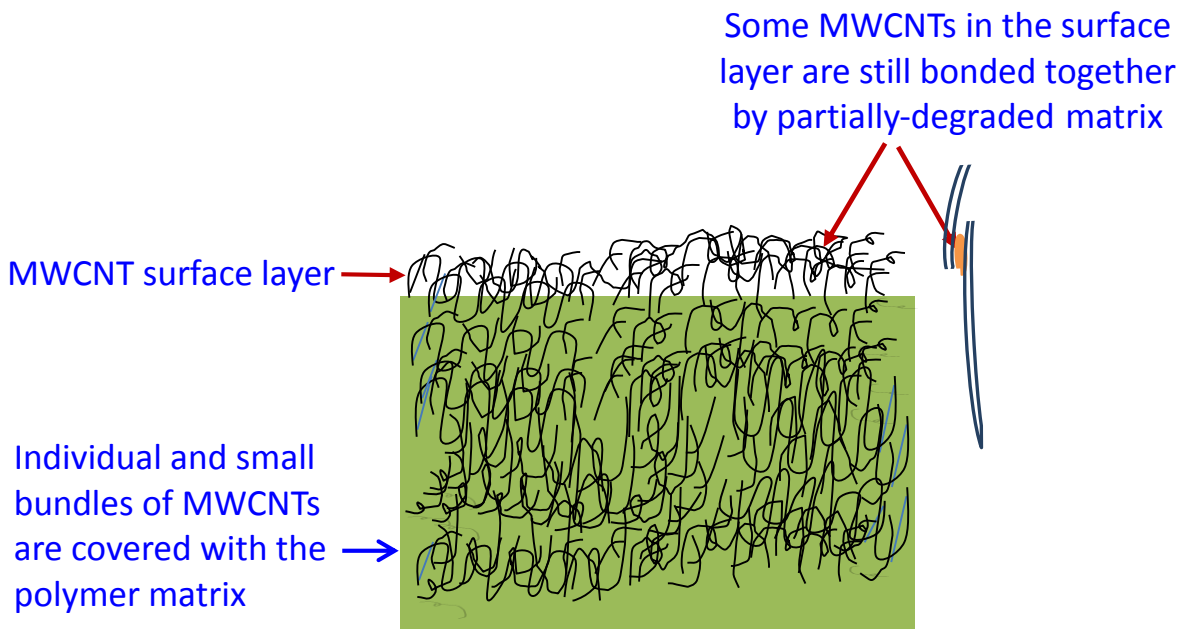
383
384 This mechanism is illustrated in Figure 7a. Although increasing amounts of MWCNTs are
385 exposed on the surface as the matrix is degraded by UV irradiation, parts of some protruding
386 MWCNTs are still embedded (anchored) in the matrix. Due to their strong adhesion with most
387 polymers, the embedded MWCNTs are not likely to leave the nanocomposite surface without
388 breaking the matrix. The strong MWCNT-polymer adhesion is due to the similarity of surface free
389 energies between these two materials. MWCNTs have a surface free energy (γ^s) of approximately
390 45.3 mJ/m² [50], which is similar to that of amine-cured epoxy (46.2 mJ/m²) [51] and higher than

391 that of most common polymers [52]. A filler will be readily wetted (low contact angle) by a matrix
392 when the surface energy of the filler is similar to or higher than that of the matrix resin. Therefore,
393 MWCNTs should form strong bonds with most polymers [50, 53]. For the bisphenol A-based
394 epoxy matrix used in this study, the adhesion is enhanced by the π - π interactions between the
395 MWCNT surfaces and the aromatic units in the epoxy resin [54, 55]. Such interactions have been
396 found to result in approximately 30 % and 44 % higher interfacial fracture energy and bonding
397 strength (pull-off), respectively, between MWCNTs and epoxy than those between MWCNTs and
398 non-aromatic polymers [55].

399



414 Figure 7a



435 Figure 7b

436

437 **Figure 7.** Schematic figures showing two of the four likely mechanisms responsible for the

438 release resistance of UV-induced MWCNT surface layer; a) matrix-embedded MWCNT, and b)

439 MWCNT are bonded by partially-degraded matrix.

440

441

442 3.4.2. CNT Entanglements

443 Another reason for the strong release resistance of the MWCNT surface layer is attributed
444 to their entanglement characteristics. As seen in Figure 4, the MWCNT surface layer appears as a
445 dense, entangled network. Similar entangled networks have been observed for MWCNT
446 accumulation on the sample surface of other MWCNT polymer nanocomposites exposed to
447 weathering environments [14, 17, 28, 31, 37]. The entangled MWCNT network formation is not
448 unique to the surface layer formed by the UV irradiation of nanocomposites, but is generally
449 observed in polymer nanocomposites made of both SWCNTs and MWCNT, even at low loadings
450 [56, 57]. The main driving force for CNT entanglements is their large aspect ratio and the van der
451 Waals interactions between different parts of the CNTs. That is, when the two ends of a CNT that
452 has a length greater than a critical length get closer, they will join to each other under the driving
453 force of van der Waals interactions, and a racket-like, folded CNT is formed [58]. Entanglement
454 is one of the main mechanisms responsible for the increase of load transfer in polymer CNT
455 composites [58], and has been modeled by different methods [57, 58]. We believe this CNT
456 entanglement provides a strong mechanical hooking that prevents individual MWCNT from
457 leaving the MWCNT surface layer, even under applied mild mechanical stress such as sonication.
458 In particular, the entanglement is likely an important mechanism to preventing some protruded
459 MWCNTs that are no longer embedded in the matrix from releasing because they still interweave
460 with the embedded ones.

461 3.4.3. Matrix-CNT Bonding in the MWCNT Surface Layer

462 Another reason that can also contribute to the release resistance of the UV-induced
463 MWCNT surface layer is the bonding between the MWCNTs and the partially-degraded matrix in

464 this layer. This is illustrated in Figure 7b, which shows some MWCNTs or their bundles in the
465 entangled MWCNT surface layer are still bonded together by residual or partially-degraded matrix
466 material. For samples with MWCNTs well dispersed in the polymer matrix, which is the case for
467 this study, previous work [42] has shown that each MWCNT or each small MWCNT bundle is
468 completely covered by the matrix. As the matrix is degraded and the MWCNT surface layer is
469 formed by irradiation, it is expected that, depending on the UV dose level, parts of some tubes or
470 their bundles in this layer are still covered with the matrix material, particularly for areas that are
471 not directly exposed to the radiation. This matrix material can provide a strong bonding between
472 two or more MWCNTs and their bundles, and can effectively reduce their possibility for release.

473 *3.4.4. van der Waals Interactions between MWCNT.*

474 The van der Waals interactions between the MWCNT can also potentially prevent them
475 from leaving the surface layer formed during UV irradiation or weathering. The van der Waals
476 interaction between two carbon nanotubes has been measured to be ≈ 500 eV/ μm [59]. This strong
477 interaction between CNTs is the main reason for their tendency to aggregate with each other and
478 the need for application of high energy mixing to disperse them in polymeric materials. When the
479 matrix in the MWCNT surface layer is completely removed by UV radiation or weathering
480 environments, the matrix-free MWCNTs would likely still stick together because of their strong
481 van der Waals interactions. Although such an interaction is weaker than that between the
482 MWCNTs and the polymer matrix, binding between the protruded, matrix-embedded MWCNTs
483 and protruded, non-embedded MWCNTs can potentially inhibit the latter from releasing from the
484 MWCNT surface layer.

485 These mechanisms for the release resistance of the MWCNTs formed on the
486 nanocomposite surface subject to UV irradiation are proposed based solely on known material
487 properties of the MWCNT and its interaction with an amine-cured epoxy. Experimental data are
488 needed using very short MWCNTs so that the entanglement phenomenon is eliminated and the
489 extent of van der Waals force interactions between CNTs is substantially reduced in both amine-
490 cured epoxy and hydrophobic polyethylene matrices to verify some of these proposed mechanisms.

491 **4. Conclusions**

492 This study has investigated the degradation of a 0.72 % MWCNT/amine-cured epoxy
493 nanocomposite exposed to UV radiation at various doses, the effects of these UV exposures on the
494 surface accumulation and release of MWCNTs, and possible mechanisms responsible for the
495 strong release resistance of the MWCNT surface layer formed on nanocomposites by UV
496 irradiation. Irradiated samples were characterized for chemical degradation, mass loss, surface
497 morphological changes, and MWCNT release using a variety of analytical techniques. The results
498 showed that, under UV radiation, the epoxy matrix underwent photodegradation that produced an
499 accumulation of MWCNTs on the surface. The MWCNT aggregated and formed a dense,
500 entangled network structure that decreased the degradation of the epoxy polymer layer underneath,
501 an identical finding to that obtained after UV irradiation of the 3.5 % MWCNT epoxy
502 nanocomposite samples. This also reduced the MWCNT surface layer growth with increasing UV
503 dose. No evidence of MWCNT release was observed during UV irradiation, even at a very high
504 dose (4865 MJ/m², equivalent to 9-month exposure). We believe such strong resistance to release
505 of the MWCNT surface layer formed by UV irradiation of polymer nanocomposites is due to four
506 main mechanisms: 1) part of the surface-exposed MWCNTs are still embedded in the polymer
507 matrix, 2) the entanglement propensity of CNTs, which mechanically hook matrix-free MWCNTs

508 with matrix-embedded MWCNT, 3) surface-exposed MWCNTs are still bonded together by
509 partially-degraded matrix, and 4) strong van der Waals interactions between matrix-free
510 MWCNTs. Additional research is needed to investigate the relative impact of these four different
511 mechanisms for different types of MWCNT polymer nanocomposites and MWCNT loadings and
512 how these mechanisms would influence the potential for CNT release after additional
513 environmental and mechanical stresses. Understanding the processes that cause the formation of
514 the MWCNT surface layer and the underlying reasons that hinder or facilitate the release of
515 MWCNTs from polymer nanocomposites exposed to weathering elements can play a critical role
516 in the design of safe, sustainable nanocomposites for applications in various industries.

517 **Disclaimer:** *Certain commercial product or equipment is described in this paper in order to*
518 *specify adequately the experimental procedure. In no case does such identification imply*
519 *recommendation or endorsement by the National Institute of Standards and Technology, nor does*
520 *it imply that it is necessarily the best available for the purpose.*

521 **Supplementary Data**

522 Supplementary data associated with this article can be found in the online version.

523 **Acknowledgements**

524 Research performed in part at the NIST Center for Nanoscale Science and Technology.

525

526 **References**

- 527 [1] Wohlleben, W.; Neubauer, N., Quantitative rates of release from weathered nanocomposites
528 are determined across 5 orders of magnitude by the matrix, modulated by the embedded
529 nanomaterial. *NanoImpact* **2016**, *1*, 39-45.
- 530 [2] Chinnappan, A.; Baskar, C.; Kim, H.; Ramakrishna, S., Carbon nanotube hybrid
531 nanostructures: future generation conducting materials. *J. Mater. Chem. A* **2016**, *4*, (24), 9347-
532 9361.
- 533 [3] Zhang, J.; Terrones, M.; Park, C. R.; Mukherjee, R.; Monthieux, M.; Koratkar, N., et al.,
534 Carbon science in 2016: Status, challenges and perspectives. *Carbon* **2016**, *98*, 708-732.
- 535 [4] Liu, Y. Y.; Zhao, J.; Zhao, L. Y.; Li, W. W.; Zhang, H.; Yu, X., et al., High Performance Shape
536 Memory Epoxy/Carbon Nanotube Nanocomposites. *ACS Appl. Mater. Interf.* **2016**, *8*, (1), 311-
537 320.
- 538 [5] Nadiv, R.; Shtein, M.; Refaeli, M.; Peled, A.; Regev, O., The critical role of nanotube shape in
539 cement composites. *Cem. Concr. Compos.* **2016**, *71*, 166-174.

540 [6] Nowack, B.; David, R. M.; Fissan, H.; Morris, H.; Shatkin, J. A.; Stintz, M., et al., Potential
541 release scenarios for carbon nanotubes used in composites. *Environ. Intl.* **2013**, *59*, (0), 1-11.

542 [7] Petersen, E. J.; Zhang, L. W.; Mattison, N. T.; O'Carroll, D. M.; Whelton, A. J.; Uddin, N., et
543 al., Potential release pathways, environmental fate, and ecological risks of carbon nanotubes.
544 *Environ. Sci. Technol.* **2011**, *45*, (23), 9837-9856.

545 [8] Gorham, J. M.; Nguyen, T.; Bernard, C.; Stanley, D.; Holbrook, R. D., Photo-induced surface
546 transformations of silica nanocomposites. *Surf. Interface Anal.* **2012**, *44*, (13), 1572-1581.

547 [9] Nguyen, T.; Pellegrin, B.; Bernard, C.; Rabb, S.; Stutzman, P.; Gorham, J. M., et al.,
548 Characterization of Surface Accumulation and Release of Nanosilica During Irradiation of
549 Polymer Nanocomposites by Ultraviolet Light. *J. Nanosci. Nanotechnol.* **2012**, *12*, (8), 6202-6215.

550 [10] Gottschalk, F.; Nowack, B., The release of engineered nanomaterials to the environment. *J.*
551 *Environ. Monit.* **2011**, *13*, (5), 1145-1155.

552 [11] Asmatulu, R.; Mahmud, G. A.; Hille, C.; Misak, H. E., Effects of UV degradation on surface
553 hydrophobicity, crack, and thickness of MWCNT-based nanocomposite coatings. *Progress in*
554 *Organic Coatings* **2011**, *72*, (3), 553-561.

555 [12] Wohlleben, W.; Vilar, G.; Fernandez-Rosas, E.; Gonzalez-Galvez, D.; Gabriel, C.; Hirth, S.,
556 et al., A pilot interlaboratory comparison of protocols that simulate aging of nanocomposites and
557 detect released fragments. *Environ. Chem.* **2014**, *11*, (4), 402-418.

558 [13] Froggett, S. J.; Clancy, S. F.; Boverhof, D. R.; Canady, R. A., A review and perspective of
559 existing research on the release of nanomaterials from solid nanocomposites. *Part. Fibre Toxicol.*
560 **2014**, *11*.

561 [14] Ging, J.; Tejerina-Anton, R.; Ramakrishnan, G.; Nielsen, M.; Murphy, K.; Gorham, J. M., et
562 al., Development of a conceptual framework for evaluation of nanomaterials release from
563 nanocomposites: Environmental and toxicological implications. *Sci. Tot. Environ.* **2014**, *473*, 9-
564 19.

565 [15] Duncan, T. V., Release of Engineered Nanomaterials from Polymer Nanocomposites: the
566 Effect of Matrix Degradation. *ACS Appl. Mater. Interf.* **2015**, *7*, (1), 20-39.

567 [16] Schlagenhauf, L.; Nüesch, F.; Wang, J., Release of Carbon Nanotubes from Polymer
568 Nanocomposites. *Fibers* **2014**, *2*, (2), 108.

569 [17] Fernández-Rosas, E.; Vilar, G.; Janer, G.; González-Gálvez, D.; Puentes, V.; Jamier, V., et al.,
570 Influence of nanomaterials compatibilization strategies in polyamide nanocomposite properties
571 and nanomaterials release during the use phase. *Environ. Sci. Technol.* **2016**, *50*, (5), 2584-2594.

572 [18] Reed, R. B.; Goodwin, D. G.; Marsh, K. L.; Capracotta, S. S.; Higgins, C. P.; Fairbrother, D.
573 H., et al., Detection of single walled carbon nanotubes by monitoring embedded metals. *Environ.*
574 *Sci. Proc. Imp.* **2013**, *15*, (1), 204-213.

575 [19] Petersen, E. J.; Diamond, S. A.; Kennedy, A. J.; Goss, G. G.; Ho, K.; Lead, J., et al., Adapting
576 OECD Aquatic Toxicity Tests for Use with Manufactured Nanomaterials: Key Issues and
577 Consensus Recommendations. *Environ. Sci. Technol.* **2015**, *49*, (16), 9532-9547.

578 [20] Edgington, A. J.; Petersen, E. J.; Herzing, A. A.; Podila, R.; Rao, A.; Klaine, S. J., Microscopic
579 investigation of single-wall carbon nanotube uptake by *Daphnia magna*. *Nanotoxicology* **2014**, *8*,
580 (S1), 2-10.

581 [21] Godwin, H.; Nameth, C.; Avery, D.; Bergeson, L. L.; Bernard, D.; Beryt, E., et al.,
582 Nanomaterial Categorization for Assessing Risk Potential To Facilitate Regulatory Decision-
583 Making. *ACS Nano* **2015**, *9*, (4), 3409-3417.

584 [22] Aschberger, K.; Johnston, H. J.; Stone, V.; Aitken, R. J.; Hankin, S. M.; Peters, S. A. K., et
585 al., Review of carbon nanotubes toxicity and exposure-Appraisal of human health risk assessment
586 based on open literature. *Crit. Rev. Toxicol.* **2010**, *40*, (9), 759-790.

587 [23] Schlagenhauf, L.; Kianfar, B.; Buerki-Thurnherr, T.; Kuo, Y. Y.; Wichser, A.; Nuesch, F., et
588 al., Weathering of a carbon nanotube/epoxy nanocomposite under UV light and in water bath:
589 impact on abraded particles. *Nanoscale* **2015**, *7*, (44), 18524-18536.

590 [24] Selck, H.; Handy, R. D.; Fernandes, T. F.; Klaine, S. J.; Petersen, E. J., Nanomaterials in the
591 aquatic environment: A European Union–United States perspective on the status of ecotoxicity
592 testing, research priorities, and challenges ahead. *Environ. Toxicol. Chem.* **2016**, *35*, (5), 1055-
593 1067.

594 [25] Bello, D.; Wardle, B. L.; Yamamoto, N.; deVilloria, R. G.; Garcia, E. J.; Hart, A. J., et al.,
595 Exposure to nanoscale particles and fibers during machining of hybrid advanced composites
596 containing carbon nanotubes. *J. Nano. Res.* **2009**, *11*, (1), 231-249.

597 [26] Bello, D.; Wardle, B. L.; Zhang, J.; Yamamoto, N.; Santeufemio, C.; Hallock, M., et al.,
598 Characterization of Exposures To Nanoscale Particles and Fibers During Solid Core Drilling of
599 Hybrid Carbon Nanotube Advanced Composites. *Int. J. Occ. Saf. Environ. Health* **2010**, *16*, (4),
600 434-450.

601 [27] Cena, L. G.; Peters, T. M., Characterization and control of airborne particles emitted during
602 production of epoxy/carbon nanotube nanocomposites. *J. Occ. Environ. Hyg.* **2011**, *8*, (2), 86-92.

603 [28] Wohlleben, W.; Brill, S.; Meier, M. W.; Mertler, M.; Cox, G.; Hirth, S., et al., On the Lifecycle
604 of Nanocomposites: Comparing Released Fragments and their In-Vivo Hazards from Three
605 Release Mechanisms and Four Nanocomposites. *Small* **2011**, *7*, (16), 2384-2395.

606 [29] Huang, G. N.; Park, J. H.; Cena, L. G.; Shelton, B. L.; Peters, T. M., Evaluation of airborne
607 particle emissions from commercial products containing carbon nanotubes. *J. Nano. Res.* **2012**,
608 *14*, (11).

609 [30] Schlagenhauf, L.; Chu, B. T. T.; Buha, J.; Nuesch, F.; Wang, J., Release of Carbon Nanotubes
610 from an Epoxy-Based Nanocomposite during an Abrasion Process. *Environ. Sci. Technol.* **2012**,
611 *46*, (13), 7366-7372.

612 [31] Hirth, S.; Cena, L.; Cox, G.; Tomović, Ž.; Peters, T.; Wohlleben, W., Scenarios and methods
613 that induce protruding or released CNTs after degradation of nanocomposite materials. *J. Nano.*
614 *Res.* **2013**, *15*, (4), 1-15.

615 [32] Wohlleben, W.; Meier, M. W.; Vogel, S.; Landsiedel, R.; Cox, G.; Hirth, S., et al., Elastic
616 CNT–polyurethane nanocomposite: synthesis, performance and assessment of fragments released
617 during use. *Nanoscale* **2013**, *5*, (1), 369-380.

618 [33] Schlagenhauf, L.; Buerki-Thurnherr, T.; Kuo, Y. Y.; Wichser, A.; Nuesch, F.; Wick, P., et
619 al., Carbon Nanotubes Released from an Epoxy-Based Nanocomposite: Quantification and
620 Particle Toxicity. *Environ. Sci. Technol.* **2015**, *49*, (17), 10616-10623.

621 [34] Boonruksa, P.; Bello, D.; Zhang, J. D.; Isaacs, J. A.; Mead, J. L.; Woskie, S. R.,
622 Characterization of Potential Exposures to Nanoparticles and Fibers during Manufacturing and
623 Recycling of Carbon Nanotube Reinforced Polypropylene Composites. *Ann. Occup. Hyg.* **2016**,
624 *60*, (1), 40-55.

625 [35] Wohlleben, W.; Meyer, J.; Muller, J.; Muller, P.; Vilsmeier, K.; Stahlmecke, B., et al., Release
626 from nanomaterials during their use phase: combined mechanical and chemical stresses applied to
627 simple and multi-filler nanocomposites mimicking wear of nano-reinforced tires. *Environmental*
628 *Science-Nano* **2016**, *3*, (5), 1036-1051.

629 [36] Wohlleben, W.; Kingston, C.; Carter, J.; Sahle-Demessie, E.; Vázquez-Campos, S.; Acrey,
630 B., et al., NanoRelease: Pilot interlaboratory comparison of a weathering protocol applied to
631 resilient and labile polymers with and without embedded carbon nanotubes. *Carbon* **2017**, *113*,
632 346-360.

633 [37] Petersen, E. J.; Lam, T.; Gorham, J. M.; Scott, K. C.; Long, C. J.; Stanley, D., et al., Methods
634 to assess the impact of UV irradiation on the surface chemistry and structure of multiwall carbon
635 nanotube epoxy nanocomposites. *Carbon* **2014**, *69*, 194-205.

636 [38] Kamal, M.; Huang, B., Natural and Artificial Weathering of Polymers. In *Handbook of*
637 *Polymer Degradation*, Hamid, S.; Amin, M.; Maadhah, A., Eds. Marcel Dekker: New York, 1992;
638 pp 127-178.

639 [39] Chin, J.; Byrd, E.; Embree, N.; Garver, J.; Dickens, B.; Finn, T., et al., Accelerated UV
640 weathering device based on integrating sphere technology. *Rev. Sci. Instrum.* **2004**, *75*, (11), 4951-
641 4959.

642 [40] Singh, D.; Sotiriou, G. A.; Zhang, F.; Mead, J.; Bello, D.; Wohlleben, W., et al., End-of-life
643 thermal decomposition of nano-enabled polymers: effect of nanofiller loading and polymer matrix
644 on by-products. *Environ. Sci.: Nano* **2016**.

645 [41] O'Carroll, D. M.; Liu, X.; Mattison, N. T.; Petersen, E. J., Impact of diameter on carbon
646 nanotube transport in sand. *J. Coll. Interf. Sci.* **2013**, *390*, 96-104.

647 [42] Banerjee, D.; Nguyen, T.; Chuang, T.-J., Mechanical properties of single-walled carbon
648 nanotube reinforced polymer composites with varied interphase's modulus and thickness: A finite
649 element analysis study. *Computational Materials Science* **2016**, *114*, 209-218.

650 [43] Gu, X.; Dickens, B.; Stanley, D.; Byrd, W. E.; Nguyen, T.; Vaca-Trigo, I., et al., Linking
651 Accelerating Laboratory Test with Outdoor Performance Results for a Model Epoxy Coating
652 System. In *Service Life Prediction of Polymeric Materials*, Martin, J. W.; Ryntz, R. A.; Chin, J.;
653 Dickie, R. A., Eds. Springer: New York, 2008.

654 [44] Vaca-Trigo, I.; Meeker, W. Q., A Statistical model for linking field and laboratory exposure
655 results for a model coating. In *Service Life Prediction of Polymeric Materials*, Martin, J. W.;
656 Ryntz, R. A.; Chin, J.; Dickie, R. A., Eds. Springer: New York, 2008.

657 [45] Zhao, M.; Gu, X.; Lowther, S. E.; Park, C.; Jean, Y. C.; Nguyen, T., Subsurface
658 characterization of carbon nanotubes in polymer composites via quantitative electric force
659 microscopy. *Nanotechnol.* **2010**, *21*, (22), 225702.

660 [46] Najafi, E.; Shin, K., Radiation resistant polymer-carbon nanotube nanocomposite thin films.
661 *Colloids Surf., A* **2005**, *257-58*, 333-337.

662 [47] Gorham, J. M.; Woodcock, J. W.; Scott, K. C., NIST SP 1200-10: Challenges, Strategies and
663 Opportunities for Measuring Carbon Nanotubes within a Polymer Composite by X-ray
664 Photoelectron Spectroscopy. 2015; p 13.

665 [48] Nguyen, T.; Wohlleben, W.; Sung, L. P., Chap. 14. In *Mechanisms of Aging and Release from*
666 *Weathered Nanocomposites*, Taylor & Francis: Boca Raton, FL, 2014.

667 [49] Long, C. J.; Orloff, N. D.; Twedt, K. A.; Lam, T.; Vargas-Lara, F.; Zhao, M., et al., Giant
668 surface conductivity enhancement in a carbon nanotube composite by ultraviolet light exposure.
669 *ACS Appl. Mater. Interf.* **2016**, *8*, (35), 23230-23235.

670 [50] Nuriel, S.; Liu, L.; Barber, A. H.; Wagner, H. D., Direct measurement of multiwall nanotube
671 surface tension. *Chem. Phys. Let.* **2005**, *404*, (4-6), 263-266.

672 [51] Kinloch, A. J., Ed., In *Durability of Structural Adhesives*, Applied Science: N.Y., 1983; p 10.

673 [52] Wu, S., In *Polymer Interface and Adhesion*, Marcel Dekker, Inc.: New York, 1982; pp 169-
674 180.

675 [53] Wagner, H. D.; Vaia, R. A., Nanocomposites: issues at the interface. *Materials Today* **2004**,
676 7, (11), 38-42.

677 [54] Yang, M. J.; Koutsos, V.; Zaiser, M., Interactions between polymers and carbon nanotubes:
678 A molecular dynamics study. *J. Phys. Chem. B* **2005**, *109*, (20), 10009-10014.

679 [55] Chen, X.; Zhang, L.; Zheng, M.; Park, C.; Wang, X.; Ke, C., Quantitative nanomechanical
680 characterization of the van der Waals interfaces between carbon nanotubes and epoxy. *Carbon*
681 **2015**, *82*, 214-228.

682 [56] Zhao, M.; Ming, B.; Kim, J.-W.; Gibbons, L. J.; Gu, X.; Nguyen, T., et al., New insights into
683 subsurface imaging of carbon nanotubes in polymer composites via scanning electron microscopy.
684 *Nanotechnol.* **2015**, *26*, (8).

685 [57] Vargas-Lara, F.; Douglas, J. F., Confronting the complexity of CNT materials. *Soft Matter*
686 **2015**, *11*, (24), 4888-4898.

687 [58] Lu, W.; Chou, T.-W., Analysis of the entanglements in carbon nanotube fibers using a self-
688 folded nanotube model. *Journal of the Mechanics and Physics of Solids* **2011**, *59*, (3), 511-524.

689 [59] Girifalco, L. A.; Hodak, M.; Lee, R. S., Carbon nanotubes, buckyballs, ropes, and a universal
690 graphitic potential. *Phys. Rev. B: Condens. Matter* **2000**, *62*, (19), 13104-13110.